JOURNAL OF CATALYSIS 128, 161–185 (1991)

Microstructure and Reactivity of Pt–Ce and Rh–Ce Particles on Silica[1]

T. CHOJNACKI,[2] K. KRAUSE,[3] AND L. D. SCHMIDT

Department of Chemical Engineering and Materials Science, University of Minnesota, Minneapolis, Minnesota 55455

Received June 12, 1990; revised September 5, 1990

The interactions of Ce with 20 to 200-Å-diameter particles of Pt and Rh on planar SiO_2 are examined using transmission electron microscopy (TEM) and reactivity measurements following treatment in H_2 and O_2 atmospheres. Samples are transferred repeatedly between furnace and TEM so that the time evolution of the microstructures of individual particles can be observed. Upon heating Pt–Ce in H_2 at 650°C, Ce forms a thin amorphous film on the SiO_2, and the only crystalline phase observed is Pt metal for low Ce loadings. Pt particle sizes are approximately the same as without Ce, but all Pt particles are round and contain many internal defects, while all particles form single crystal cubes without Ce. For high Ce loadings a phase is detected with a diffraction pattern of cerium hydride, and dark field imaging shows that this forms as cubes near the Pt particles. Heating in O_2 causes the Ce to convert to CeO_2 particles which form around the Pt particles. When Rh–Ce is heated in H_2, a thin film of cerium forms on the SiO_2. At high Ce loadings, diffraction patterns which appear to be $CeH_{2.53}$ are observed. The Rh particles contain more defects and show less faceting than without Ce. Heating in O_2 at high Ce loadings causes Ce from the film to coalesce and form large, flat (>1000 Å diameter and ~100 Å thick) CeO_2 particles. Upon reduction in H_2 at 600–750°C, these particles disperse very slowly and may form compounds with the SiO_2. It is also observed that Rh catalyzes reduction of adjacent CeO_2 back to Ce because holes form in the CeO_2 near Rh particles. The oxidation-reduction cycle results in a redispersion of the Rh with Ce present. Reactivities of Rh–Ce catalysts in CO hydrogenation and in ethane hydrogenolysis were also measured. For CO hydrogenation, Ce increases activity by a factor of ~30, and the selectivity shifts toward higher alkanes and alkenes. For ethane hydrogenolysis, it was found that activities increase upon addition of Ce, but activities are affected more by pretreatment in H_2 or O_2 than by Ce addition.

INTRODUCTION

Pt and Rh catalyst particles are uniquely capable of the simultaneous oxidation of CO and hydrocarbons and the reduction of NO in automotive exhaust catalyst, and Ce is an important additive for these catalysts. Addition of Ce has been suggested (*1–3*) to promote the water–gas shift reaction, to provide storage of oxygen in the varying environment of the converter, to prevent thermally induced sintering of the alumina support, and to increase the dispersion of Pt and Rh (*1*).

Recently, Ce has been reported to be a promoter of Rh/SiO_2 for ethanol production in the H_2 + CO reaction while inhibiting the production of acetaldehyde and hydrocarbons (*4*). Investigations of CO hydrogenation by Rh promoted by or supported on several rare earth oxides showed that the rare earth increases the total rate and significantly shifts selectivity toward oxygenates (*5, 6*). In a study of CO and hydrocarbon oxidation over Pt and Rh on γ-Al_2O_3, CeO_2 was found to alter rates and kinetics in these reaction (*7*). Several studies have

[1] This research partially sponsored by NSF under Grant CBT8822745.

[2] Present address: Cray Research, Chippewa Falls, WI.

[3] This material is based upon work supported under a National Science Foundation Graduate Fellowship.

0021-9517/91 $3.00

TABLE 1

Possible and Observed Phases and Compounds in the Pt–Ce and Rh–Ce Systems†

Metal	H_2 Treatment	O_2 Treatment
Pt*	CePt (ortho)	CeO (fcc)
	$CePt_2$ (fcc)	Ce_2O_3 (hex)
	Ce_3Pt_2 (fcc)	CeO_2 (fcc)*
	$CePt_3$ (fcc)[a]	
	Ce_7Pt_3 (hex)[b]	
	Ce_3Pt_4 (rhom)[c]	
	$CePt_5$ (hex)	
	CeH_x (fcc)[d]	
	CeH_2 (fcc)*	
	$CeH_{2.53}$ (tet)[e]	
	Ce (many)	
Rh*#	CeRh (ortho)*	CeO#
	Ce_3Rh[f]	Ce_2O_3
	$CeRh_2$ (cubic)	CeO_2*,#
	$CeRh_3$[f]	$CeRhO_3$ (ortho)
	Ce_4Rh_3[f]	RhO_2 (tet)
	Ce_5Rh_3[f]	Rh_2O_3 (ortho, hex)*
	Ce_5Rh_4 (ortho)	
	CeH_x	
	CeH_2*	
	$CeH_{2.53}$#	
	Ce#	

* Phases observed in samples where Ce was added from salt.

\# Phases observed in samples where Ce was added by vacuum evaporation.

† Data from ASTM, X-ray powder diffraction files except for:

[a] Harris, I. R., *J. Less Com. Metals* **14,** 459 (1968).

[b] LeRoy, J. Moreau, J-M., and Piccard, D., *Acta Cryst.* **B34,** 9 (1978).

[c] Palenzona, A., *J. Less Com. Metals* **53,** 133 (1977).

[d] Pearson, W. B., "Handbook of Lattice Spacings and Structures of Metals," Vol. 2, Pergamon, New York, pp. 1403–1405 (1967).

[e] Tellefsen *et al.*, *J. Less Com. Metals* **110,** 107 (1985).

[f] Ghassen, H., and Raman, A., *Z. Metallkunde* **64,** 197 (1973).

shown that the presence of Ce in Pt and Rh on SiO_2 and Al_2O_3 retarded metal sintering as measured by infrared spectroscopy (*8*) and by CO adsorption (*9*).

The analysis of Pt–Ce and Rh–Ce is complicated by the existence of many intermetallic, hydride, oxide, silicate, and silicide phases. In addition, Ce metal can form several crystal structures. Table 1 lists many of the possible phases and their crystal structures. Phases marked with an "*" were observed in samples in which Ce was added from salt solution and phases marked with a "#" were observed in Rh–Ce samples where the Ce was added by vacuum evaporation. Additional amorphous phases which can not be deteced by electron diffraction could, of course, also have been present.

This work involves the direct observation by TEM and electron diffraction of the effect of gas treatments on the shape and structure of Pt–Ce and Rh–Ce systems supported on silica. TEM allows the direct observation of the particles shapes in these systems within the resolution of the microscope, while electron diffraction provides information about the phases formed between Ce and the noble metal of each system. In particular, we are interested in the effects of heating in reducing and oxidizing atmospheres on these interactions.

We note that these experiments are on rather large (50 to 200-Å diameter) metal particles compared to many supported catalysts. Conditions used here are also more extreme than encountered in many catalysts in that we heat up to 750°C and use either pure H_2 or O_2 atmospheres. Thus, while these experiments suggest behavior expected in real catalysts, these microstructures are an exaggeration of those to be expected in real systems.

We have also studied the effects of Ce addition to Rh/SiO_2 on ethane hydrogenolysis activity and CO hydrogenation activity and selectivity. By adding the Ce before or after dispersion of the Rh, the effect of Ce on the dispersion of Rh particles can be examined. The effects on reactivity of heating in the same reducing and oxidizing environments as for TEM were investigated.

TEM EXPERIMENTAL

Pt–Ce and Rh–Ce samples for TEM were prepared by depositing metal and Ce on planar SiO_2 films on a gold microscope grid.

SiO_2 films were prepared by vacuum depositing ~200 Å film of Si on Formvar film on a gold microscope grid and heating in O_2 at 600°C to remove the polymer and oxidize the Si to SiO_2. Pt and Rh particles were formed by vacuum depositing 15- to 20-Å films of the metals and heating in H_2 at ~600°C to form particles. Ce was added by preparing $Ce(NO_3)_3 \cdot 6H_2O$ solutions diluted so that one 5-μl drop of solution would deposit the equivalent of 10 Å of Ce on a 3-mm-diameter TEM sample grid. In some experiments, Ce was added by vacuum deposition of cerium followed by heating in H_2 to reduce the oxide and disperse the film. This method resulted in a more uniform distribution of Ce and allowed samples to be prepared with several different loadings on the same TEM grid.

Samples were treated in a quartz tube furnace with the gases flowing at a rate of ~50 cc/min. High-purity hydrogen and oxygen were used without further treatment. TEM was performed on a JOEL 100CX (3.5-Å line resolution) and on a Philips CM 30 (1.4 Å) microscope. The same regions of samples could be treated, examined, retreated, and reexamined so that the morphological changes of individual particles could be examined.

The contrast of the TEM image is proportional to the electron density which is roughly proportional to the atomic numbers of the elements. These are 78, 58, 45, 16, and 8 for Pt, Ce, Rh, Si, and O, respectively, and therefore for comparable thicknesses and orientations Pt will have a higher contrast in Pt–Ce, Ce will have a higher contrast in Rh–Ce, and the SiO_2 film produces little electron scattering.

We used electron diffraction to identify crystalline phases and dark field imaging of particular diffraction rings to determine the locations of particular phases. We especially want to identify crystalline phases of Ce compounds which have low contrast, are frequently present as small particles (with consequent diffraction line broadening), and may form several crystalline and amorphous phases simultaneously. Selected area and convergent beam diffraction were used to identify the location of phases in the Rh–Ce system since dark field imaging from a single reflection was complicated by the large number of phases.

To observe low contrast structures in TEM images and in diffraction patterns, we also used the technique of unsharp masking (*10*). In this technique one prepares an out-of-focus positive image of the negative and prints a superposition of the two images so that high contrast features are reduced in intensity to permit observation of weaker features. Using unsharp masking, we can observe features which have intensities only a few percent of major features.

We examined many samples with different loadings and methods of preparation and treatment. We show here micrographs of only several samples so that we can display the *time evolution of individual regions of a single sample*. All results reported were reproduced on several samples, and in no cases were results significantly different from results shown and described. Contamination was a problem with salt-deposited multimetal samples, and in some samples complex structures and diffraction rings were observed, especially in early experiments. We observed no unidentifiable diffraction rings from carefully prepared samples.

The same samples were examined repeatedly by cooling in the furnace in flowing gas and transferring the sample across the laboratory to the TEM where the same particles were located. We have shown previously that Pt (*11*) and Rh (*12*) do not oxidize significantly in air at room temperature, and even reactive metals such as Ni (*13*) and Mo (*14*) remain metallic when 100-Å particles are transferred in air. However, Ce is highly reactive in O_2 and may not form a protective oxide film as do Ni and Mo; therefore intermetallic compounds and Ce metal or hydride might be formed by treating in H_2 but decompose

during transfer for TEM. We note however that we observe all of these phases in some situations.

TEM RESULTS

Identification of the valence state of Ce in observed oxides or hydrides is important in determining the role Ce may play in storing oxygen under oxygen-rich conditions for use under oxygen-deficient conditions. Ce can form three oxides (CeO, Ce_2O_3, and CeO_2) each having a well-characterized chemistry and crystal structure. Survey of the literature, however, indicates that Ce can form many fcc hydrides. In CeH_x, as x increases from 0 to 3 the lattice constant increases from ~5.13 Å, passes through a maximum at $x \approx 1.7$ of ~5.57 Å, and then decreases to ~5.52 Å (*15*). A tetragonal $CeH_{2.53}$ phase which is very nearly cubic (a = 5.543, c = 5.561 Å) has also been reported recently (*16*). Lattice constant measurements by electron diffraction do not have enough accuracy to determine the precise value of x in CeH_x. As discussed below, we observed two different phases identifiable as Ce hydrides. Their measured lattice constants are best fit by assignment as CeH_2 and $CeH_{2.53}$, but it should be noted that these assignments are limited by the precision of the lattice constant measurements. We also note that formation and observation of hydride phases is surprising because it requires Ce to be reduced to the zero valent state and because hydrides might be expected to be decomposed by room temperature oxidation during transfer from the oven to the TEM.

Platinum–Cerium

Figures 1 and 2 show the same set of particles on a single substrate after heating sequentially in H_2, O_2, and H_2, respectively. The three arrows in the figures identify the same particles on all micrographs. This sample had a Ce/Pt atom ratio of ~2. As shown in Fig. 1a, after heating in H_2 at 650°C for 16 hr, the Pt film breaks up to form small particles ~150 Å in diameter. Pt particle sizes are approximately the same as without Ce, although the presence of Ce metal alters the structures of the Pt in that the Pt forms particles which are highly twinned and generally round in outline although some still show faceting. This structure is quite different from that of pure Pt particles formed under similar conditions, in which structures are characteristically defect-free and cube shaped if grown in H_2 (*11*). At this Ce loading and temperature, Ce does not form any observable intermetallic compounds with Pt as might be expected from the phase diagram of Pt–Ce (*17*). Instead the Ce appears to be distributed as an amorphous but discontinuous film which can be seen as the low contrast structures throughout the field of the support (Fig. 1a).

The absence of crystalline phases of Ce for these Ce loadings is confirmed by electron diffraction which shows only extremely faint rings of a crystalline species which may be due to a Ce hydride and intense rings of Pt metal (Fig. 1b). The lattice constant of Pt is unchanged by the presence of Ce. Incomplete reduction of the Ce and the formation of CeO_2 occurs if the heating time is shorter at 650°C or if the concentration of the Ce salt is increased without extending the heating time.

Figure 2a shows the same particles as in Fig. 1a after heating in O_2 at 550°C following the initial H_2 treatment. The arrows in the figure indicate locations identical to those on Fig. 1a. It is seen that this causes the Pt

FIG. 1. (a) Micrograph of a typical sample of Pt–Ce with Ce/Pt~2 after treatment in H_2 at 650°C for 16 hr. The Pt particles have more rounded outlines and are more highly twinned than for Pt alone. A low-contrast Ce film uniformly covers the SiO_2 support. (b) The diffraction pattern shows only the fcc ring pattern of Pt metal with the first three rings labeled. No indication of a second species or of any change in the lattice constant of Pt is evident.

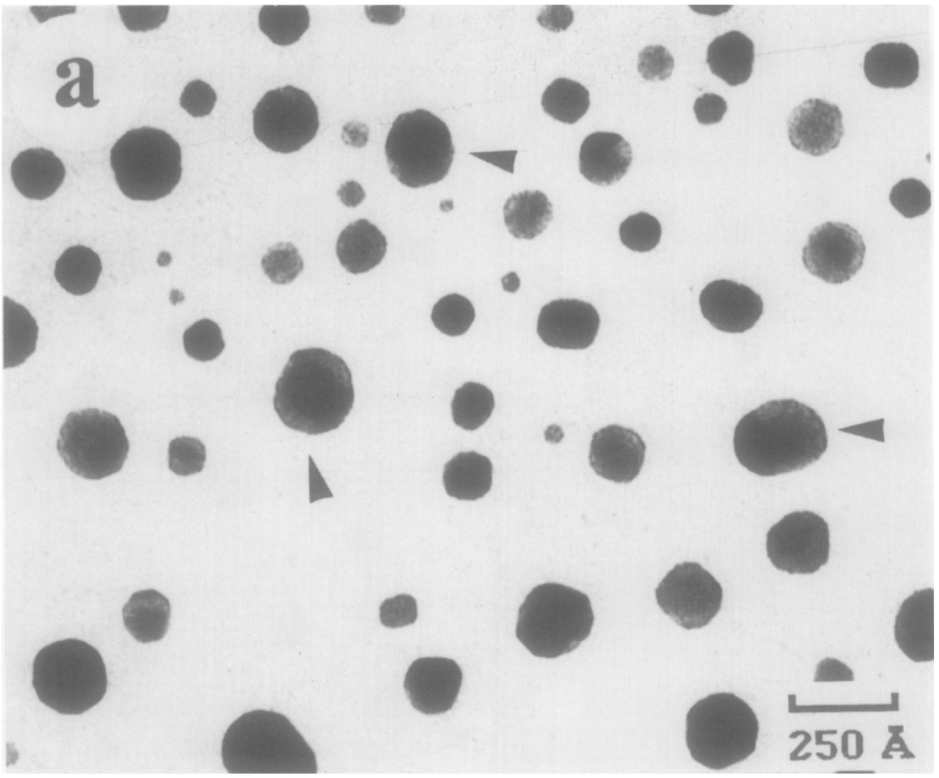
a
250 Å

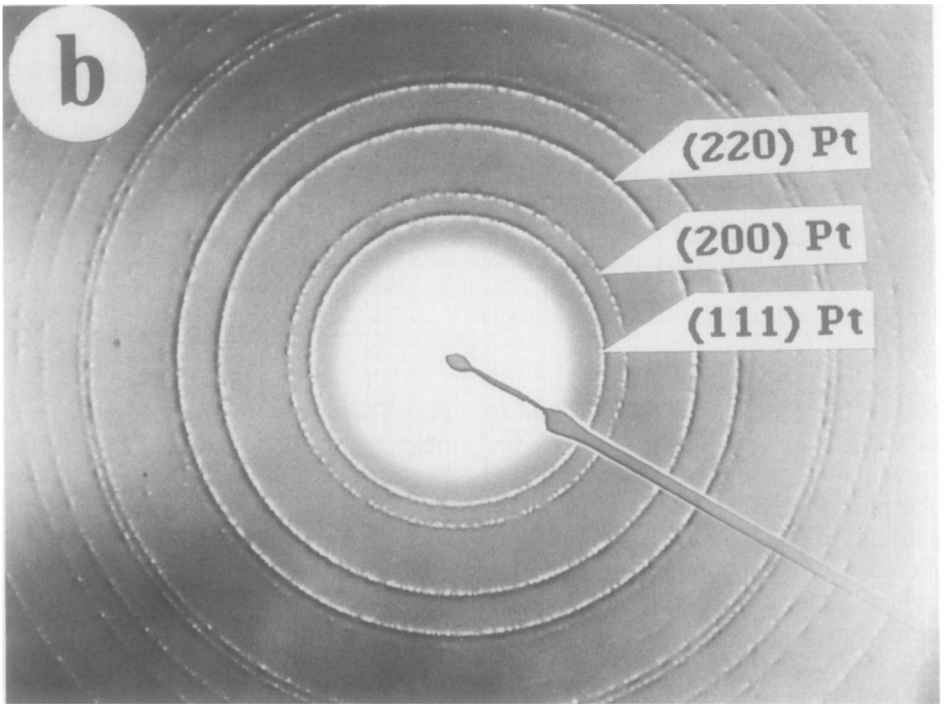
b
(220) Pt
(200) Pt
(111) Pt

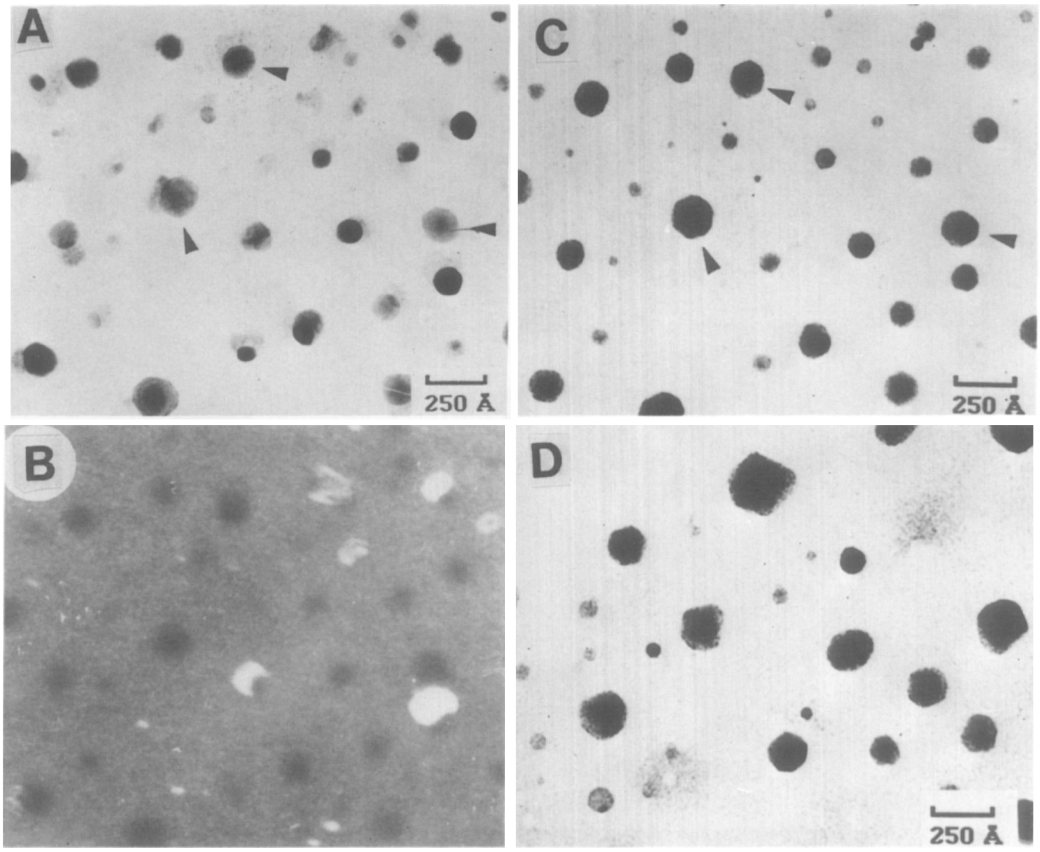

FIG. 2. (a) Micrograph of the particles shown in Fig. 1 (arrows indicate same particles in each figure) after subsequent treatment in O_2 for 1 hr at 550°C. All particles are reduced in lateral size but remain round in shape. Many of the particles have lower contrast rectangular structures adjacent to them which are CeO_2. The fine structure on the support which was a film in Fig. 1 has now transformed into small particles of CeO_2 ~25 Å in size. (b) Dark field image using the (111) reflection of CeO_2 identifies the rectangular structures adjacent to the round particles and the small ~25-Å particles as CeO^2. (c) Heating the oxidized sample of (a) in H_2 at 650°C for 1 hr causes the rectangular CeO_2 structures to disappear and the small CeO_2 particles to disappear or to transform to smallar particles ~10 Å in size. (d) After heating in H_2 for time of 5 hr, the Pt particles have sintered more extensively and the small 10-Å particles noted in (c) have increased in size.

particles to become slightly smaller and to change shape slightly. The particles also become even more rounded, similar to that seen for pure Pt (*11*).

Treatment in O_2 also causes formation of lower contrast rectangular structures of a size comparable to the parent particles which are almost always adjacent to the Pt particles (Fig. 2a). This treatment also results in the formation of small particles <25 Å throughout the field of the SiO_2 support. The number density of these small particles is less in the immediate vicinity of the larger Pt particles.

The appearance of the small particles and rectangular structures is accompanied in the diffraction pattern by the appearance of diffraction rings which can be assigned to CeO_2 (not shown). Dark field imaging using the (111) ring of the CeO_2 (Fig. 2b) confirms that both the small particles in the field of the support and the rectangular structures adja-

cent to the Pt particles are CeO_2, while the dark field image using the (111) ring of Pt (not shown) shows the large particles to be Pt metal.

When Pt–Ce samples are again treated in H_2 at 650°C for 1 hr, the CeO_2 structure is replaced by particles ~10 Å in size which are uniformly distributed throughout the field of the support. After long heating in H_2, accompanying this change in the structure of the CeO_2 particles is the loss of the CeO_2 rings in the diffraction pattern and the formation of a ring of very weak intensity assignable to the cerium hydride CeH_2 (Fig. 2c). The Pt retains its diffraction pattern and remains almost unchanged in shape.

When heating times in H_2 are extended or the amount of Ce is increased to Ce/Pt > 3 (Fig. 2d), cerium hydride begins to become discernable as the size of the small dispersed particles grows, the larger (Pt) particles sinter more, and the intensity of the rings assigned to the hydride increases relative to the Pt ring intensity in the diffraction pattern.

Rhodium–Cerium

Some differences in microstructures were observed between samples in which Ce was added from the salt and samples in which it was added by vacuum evaporation. We attribute this difference to the fact that depositions from salts are known to give very anisotropic particle distributions, while depositions by vacuum evaporation give nearly uniform distributions (*18*). The results when Ce was added by vacuum evaporation will be described first.

Figures 3 and 4 show an $H_2 \rightarrow O_2 \rightarrow H_2$ treatment sequence for four different Rh/Ce ratios *on the same TEM grid* prepared by vacuum evaporation of Rh and Ce. This sample was prepared by selectively shielding portions of the grid during depositions. Since all four loadings were on the same grid, the heat treatments and any contaminants were identical. The top micrographs are after the initial H_2 treatment at 600°C for 14 hr, the middle micrographs after 1 hr in O_2 at 600°C, and the bottom micrographs after 4 hr in H_2 at 600°C.

When only Ce is deposited on SiO_2, no particles are observed and no crystalline phases are detected by electron diffraction (Fig. 3a). The Ce spreads out over the SiO_2 as an amorphous film. The presence of Ce on the sample was confirmed by energy dispersive spectroscopy and by the formation of ~50 Å crystalline CeO_2 particles after heating in O_2 (Fig. 3b). This figure shows small CeO_2 particles dispersed throughout the sample except for areas not covered by the film. After heating in H_2 again, the CeO_2 particles disappeared and no crystalline phases were observed (Fig. 3c). Since the film was amorphous, the oxidation state of the Ce after the initial and final H_2 treatments could not be determined by electron diffraction.

Different loadings of Ce and Rh were deposited on the other three regions. The loadings were 8 Å Rh and 22 Å Ce in Figs. 3d–3f, 14 Å Rh and 2 Å Ce in Figs. 4a–4c, and 22 Å Rh and 8 Å Ce in Figs. 4d–4f. Rh metal and Ce metal phases were identified by electron diffraction in all three regions after the initial H_2 treatment. Rings best assigned as $CeH_{2.53}$ were also observed. Assignment of rings was complicated by the overlapping of reflections from different phases and the high-intensity scattering from the amorphous SiO_2. Dispersion of the particles decreased with increasing Rh loading, and the region with the highest Rh loading still showed some interconnected particles (Fig. 4d).

The micrographs taken after heating in H_2 show that the presence of Ce inhibits the formation of the characteristic hexagonal shapes (*12*) of Rh particles alone on SiO_2 and causes the formation of many twinned and multiply twinned particles that are generally round in shape. Few of the particles showed any faceting. A thin amorphous film, similar to that observed when only Ce is deposited, can be seen covering the surface in all three regions. No Rh–Ce intermetallics are observed, and the only evidence

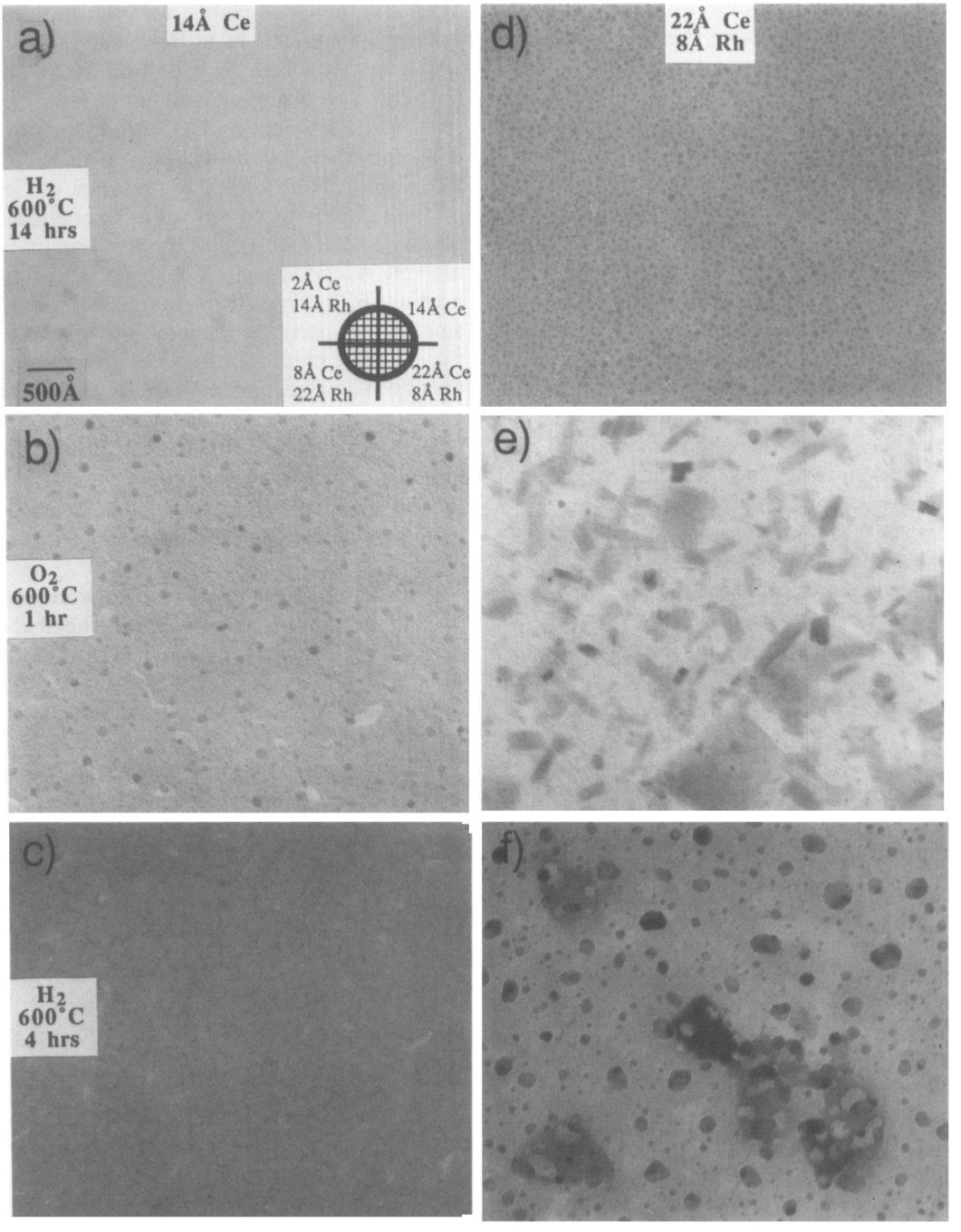

FIG. 3. Microstructures of Rh–Ce when Ce is added by vacuum evaporation. Four samples with different loadings were prepared on the same TEM grid as sketched in the inset of (a). In all panels of Figs. 3 and 4, the top micrographs are after heating in H_2 at 600°C for 14 hr, the middle micrographs are after heating in O_2 at 600°C for 1 hr, and the bottom micrographs are after heating in H_2 again at 600°C for 4 hr. (a–c) A loading of 14 Å Ce. Ce forms a continuous amorphous film which becomes somewhat granular in O_2. (d–f) show loadings of 8-Å Rh and 22-Å Ce. The Ce forms many large CeO_2 particles after heating in O_2. Reduction in H_2 produces much larger Rh particles.

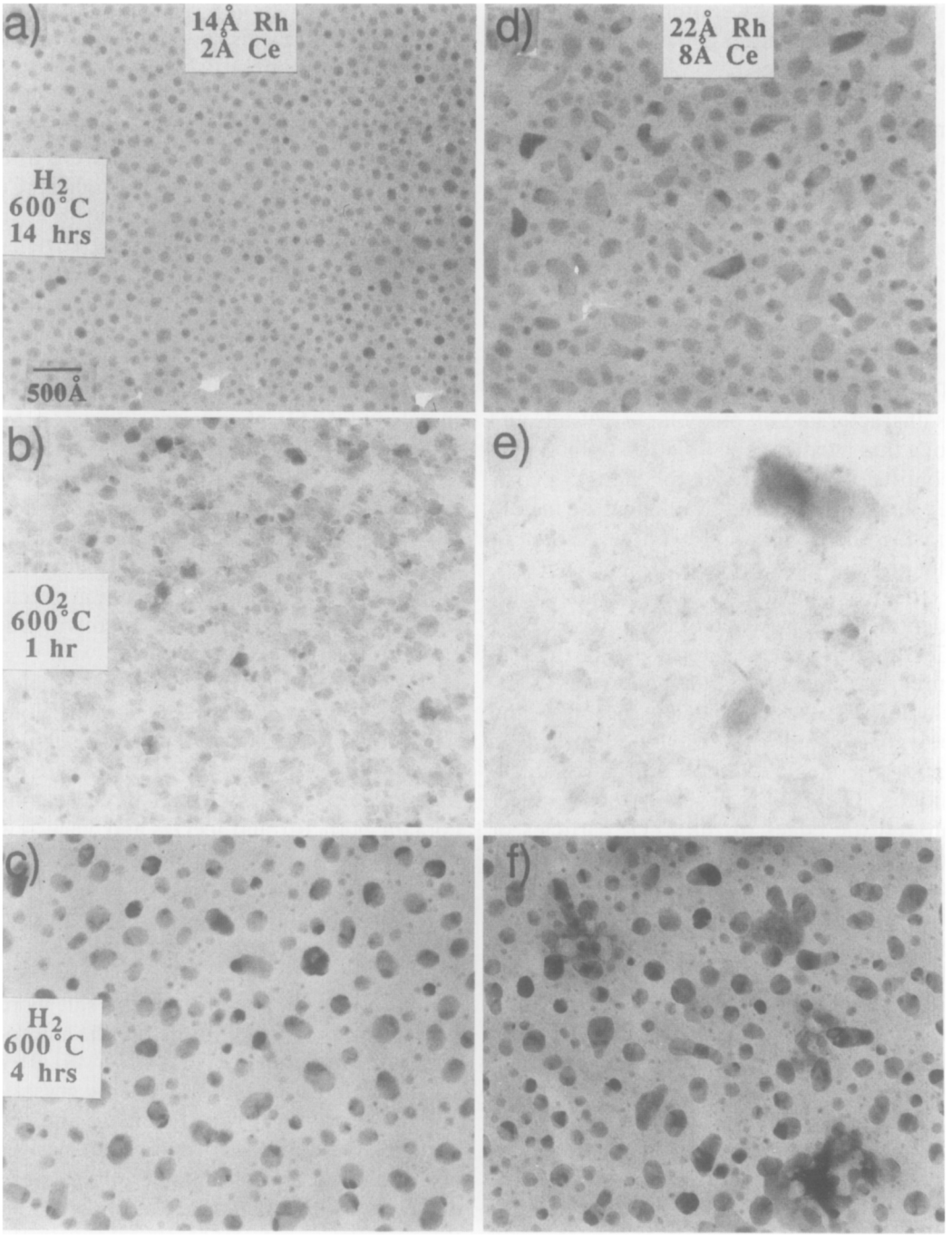

FIG. 4. Microstructures of Rh–Ce when Ce is added by vacuum evaporation. Four samples with different loadings were prepared on the same TEM grid as sketched in the inset of Fig. 3a. As in Fig. 3, the top micrographs are after heating in H_2 at 600°C for 14 hr, the middle micrographs are after heating in O_2 at 600°C for 1 hr, and the bottom micrographs are after heating in H_2 again at 600°C for 4 hr. (a–c) show loadings of 14-Å Rh and 2-Å Ce. The Ce forms small, thin CeO_2 crystals after heating in O_2. Reduction in H_2 again produces larger Rh particles as observed in Fig. 3f. (d–f) show loadings of 22-Å Rh and 8-Å Ce. At this intermediate Ce loading, the Ce forms many small, thin CeO_2 particles and some large CeO_2 particles.

of the presence of Ce after heating in H_2 in the bright field images is the change in shape of the Rh particles.

After heating in O_2, thin CeO_2 crystals, most polygonal in shape, are observed even at the lowest Ce loading (Fig. 4b). These particles show a preference to form interconnected clusters comprised of several crystals. As the Ce loading is increased, the clusters begin to coalesce and form large (500–1000 Å) particles (Fig. 4e). A film characterized by fine structure similar to that observed in the Ce-only region also appears. The microstructure at the highest Ce loading is characterized by many large crystals and long thin needles (Fig. 3e). The reduction in contrast of the particles for the two higher Ce loadings is caused by an increase in contrast of the Ce film and is not an artifact of the photographic process.

Electron diffraction after heating in O_2 identified the presence of crystalline CeO_2, CeO, and Rh metal phases. All of the features that appeared after heating in O_2 including the large particles, needles, and polygon-shaped crystals are identified as CeO_2 by single crystal diffraction techniques. The CeO is probably located in or around the edges of the CeO_2 particles or as small crystallites in the film. The high contrast particles are unoxidized Rh metal. The absence of diffraction rings from Rh oxide suggests that the Ce film is on top of the Rh preventing the O_2 from reacting with Rh, although an amorphous Rh oxide or a mixed oxide could be present. The dramatic differences in microstructure between Rh–Ce, Ce only, and Rh only (*12*) indicate significant interaction between the Rh and Ce under oxidizing conditions, although no crystalline intermetallic compounds are observed.

The TEM grid was then heated in H_2 again as shown in the lower micrographs in Figs. 3 and 4. The thin CeO_2 crystals in the region with the lowest Ce loading disappeared completely and highly defected Rh metal particles of larger size and lower number density than after the initial H_2 treatment were formed (Fig. 4c). The fine structure and small crystals disappeared from the region with intermediate Ce loading. The large particles were not completely reduced, and voids—either holes or bubbles—formed in the CeO_2 (Fig. 4f). These voids were also formed in the region with the highest Ce loading (Fig. 3f) and always appear to form adjacent to smaller, higher contrast particles identified as Rh. The sizes of particles formed after the $H_2 \rightarrow O_2 \rightarrow H_2$ sequence are similar for all three regions, but the number density increases with increased Rh loading.

After heating in H_2 the second time, Rh metal and CeO_2 phases are identified by polycrystalline diffraction and confirmed by single crystal diffraction. Figure 5b is a higher magnification image from the region with the highest Rh loading. Many particles exhibit twinned regions of greatly differing contrast. The low contrast regions are identified as CeO_2. Figure 5a is a convergent beam diffraction pattern of CeO_2 with $z = [\bar{1}11]$ taken at 0° tilt from the particle labeled with a "1" in Fig. 5b. The dark regions which tend to show some faceting such as the one marked with a "2" in Fig. 5b are Rh metal. Many particles in all three regions contain both Rh and CeO_2, and very few particles containing only Rh without CeO_2 particles nearby are observed.

We also examined the microstructure of Rh–Ce where Ce was added from the salt. When samples with Ce/Rh atom ratio <1 in which Ce was added from the salt were heated in H_2 at 650°C for 4 hr, the microstructure was similar to that observed after vacuum deposition of Ce. The only crystalline phase observed was Rh metal and the particles were generally round in shape. No crystalline Ce or intermetallic phases were detected, but fine structure was observed on the support.

At higher loadings of Ce, initial heating in H_2 resulted in the formation of rings in the diffraction pattern assignable to Rh metal and to the intermetallic compound CeRh. These particles were also round with no faceting (Fig. 6a), although many of the parti-

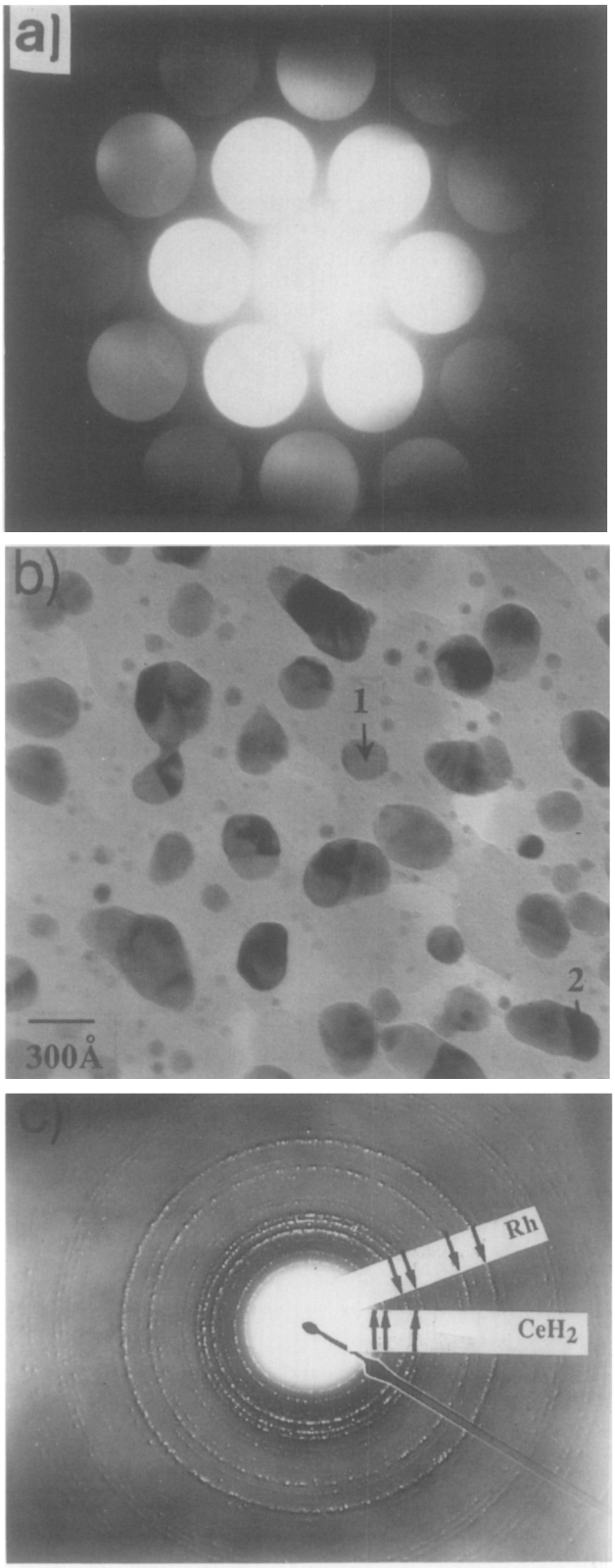

FIG. 5. (a) Convergent beam diffraction pattern from a single crystal CeO_2 particle marked by "1" in (b). Pattern is from $z = [\bar{1}11]$ and was taken at 0° tilt. (b) Higher magnification micrograph taken from the sample with the highest Rh loading after heating in H_2 after oxidation. (c) The diffraction pattern of the sample in Fig. 6c shows the presence of Rh metal and crystalline CeH_2.

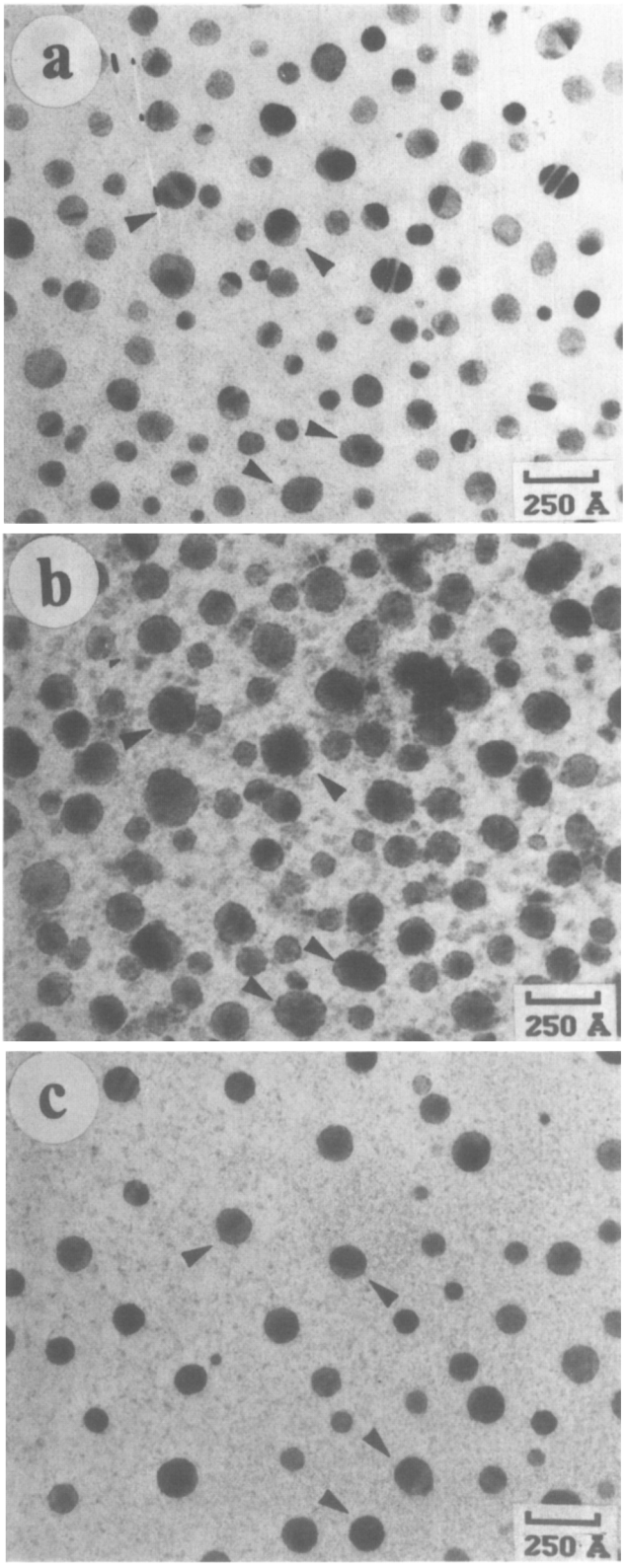
a
250 Å
b
250 Å
c
250 Å

cles contained regions of differing contrast not seen in samples with Ce/Rh < 1. Dark field imaging (not shown) using the (001) reflection of CeRh showed that the contrast variation was due to different crystals and phases and that many of the particles were composed of a Rh region and a CeRh region while others appeared to be composed only of Rh or CeRh. Fine structure can also be seen over the surface of the SiO_2.

When the Rh–Ce samples shown in Fig. 6a were treated in O_2 at 650°C for 1 hr following H_2 treatment, both Rh_2O_3 and CeO_2 were observed. However, unlike Pt–Ce samples, none of the Rh–Ce samples formed any lower contrast rectangular CeO_2 particles adjacent to Rh_2O_3, but instead the CeO_2 formed ~50 Å particles which were distributed uniformly throughout the sample similar to its parent metal (Fig. 6b).

After treatment in O_2, interspersed throughout the large structures of Rh_2O_3 are small particles of high contrast which are crystallites of unoxidized Rh metal. The presence of Rh metal is confirmed by rings in the diffraction pattern of moderate intensity assignable to Rh. Also seen in the diffraction pattern are rings of CeO_2 and Rh_2O_3. The presence of Ce thus appears to retard the rate of oxidation of Rh since pure Rh samples show total oxidation to Rh_2O_3 with no Rh metal remaining after similar treatments. This further suggests, as observed with samples prepared by vacuum evaporation of Ce, that the Ce is on top of the Rh.

When oxidized samples are then treated in H_2 at 650°C for longer than 1 hr, samples with Ce/Rh < 1 returned to approximately their original structures: Ce is dispersed uniformly over the substrate, highly twinned Rh particles form with a spherical shape, and the diffraction pattern returns to the preoxidized fcc pattern of only Rh metal.

When samples which contained Ce/Rh ≥ 2.5 were heated in H_2 at 650°C, many of the large particles disappeared altogether, while those which remained were reduced in size and show more faceting than after the initial H_2 treatment (Fig. 6c). The fine structure seen on the support after the initial H_2 treatment was replaced by ~25 Å particles. This change is also accompanied by the appearance of rings in the diffraction pattern assignable to CeH_2 and Rh metal (Fig. 5c).

Microstructures during Transformations

When heated in O_2, samples in which Ce was added from solution also formed the large CeO_2 particles observed when Ce was vacuum deposited, but longer treatment in O_2 was required. Transformations back to the initial microstructure by heating in H_2 were also much slower. This allowed us to examine in more detail the microstructures in the oxidation and reduction of Rh–Ce, and micrographs showing the effects of sequential treatments on a single region are shown in Figs. 7 and 8. Figure 7 shows micrographs of a region following reduction in H_2 at 600°C (Figs. 7a, 7b) and after oxidation in O_2 at 600°C for 2 hr (Figs. 7c, 7d). The upper panels show the same large region between a hole in the SiO_2 film and a region containing a large amount of Ce, while the

FIG. 6. Rh–Ce samples in which Ce was added from the salt after initial heating in H_2 for 16 hr at 650°C. (a) Particles formed in samples with Ce/Rh~2.5 are round in shape. Many particles are twinned and show regions of varying contrast. Fine structure can be seen over the surface of the support. (b) Treatment of the sample shown in (a) in O_2 at 550°C for 1 hr causes the Rh particles to oxidize and consequently expand, and Ce to form CeO_2 which is distributed throughout the sample. Small high-contrast particles of unoxidized Rh can be seen interspersed throughout the Rh_2O_3. (c) Micrographs of the same particles shown in (b) after heating in H_2 at 650°C for 1 hr. All larger particles have been reduced in size while many of the smaller particles have disappeared completely. Small ~25-Å particles can also be seen distributed over the surface of the support. The shapes of the particles are generally round.

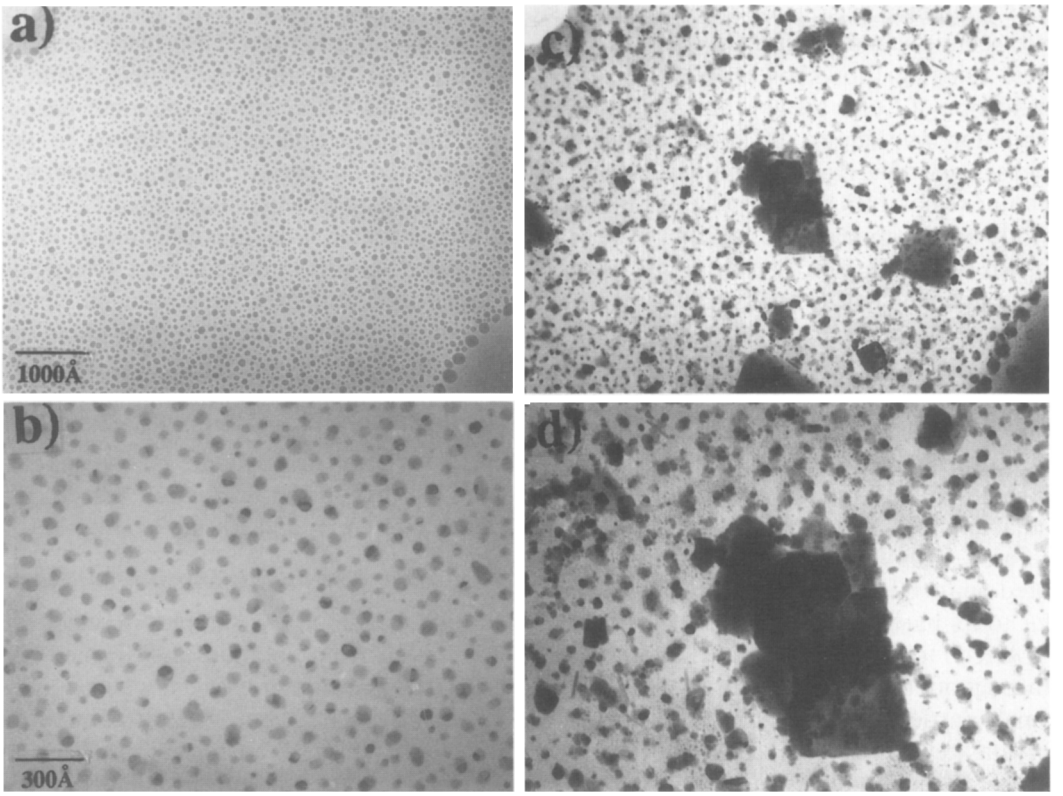

FIG. 7. Same region of an Rh–Ce sample before and after treatment in O_2 at 650°C for 2 hr. (a) and (c) were taken at low magnification to show how the same region was located after heat treatments between a hole in the SiO_2 film and a large lump of SiO_2. (b) and (d) are higher magnification images from the same areas in the center of (a) and (c). After oxidation, fine structure due to CeO_2 is visible surrounding the large CeO_2 particle.

lower panels show the same region at higher magnifications. As discussed previously, heating in H_2 produces ~200 Å particles of Rh metal; Fig. 7b shows that these are generally round in shape and most have one or more grain boundaries characteristic of internal defects associated with Ce addition to Rh.

The oxidized sample (Figs. 7c and 7d) shows large regions of lower contrast which are identified by electron diffraction to be CeO_2. These aggregate with the Rh such that most Rh particles of Figs. 7a and 7b are now larger and consist of Rh and CeO_2 phases. In several areas very large CeO_2 particles have formed: there are six regions in Fig. 7c in which the CeO_2 particles are more than 1000 Å across.

The largest of the particles in Fig. 7c is shown in Fig. 7d. This CeO_2 particle is approximately 3000 × 1000 Å and has two straight sides. Individual 100- to 200-Å particles of Rh are evident within the CeO_2 particle. The CeO_2 is not simply a three-dimensional crystal, however, because its contrast is very low, less than that of the enclosed Rh particles which cannot be more than 100 Å thick (less than their lateral dimensions). Rather, the CeO_2 forms particles which are of fairly uniform thickness and nearly flat. There are at least four distinct regions of CeO_2 with different contrast within this par-

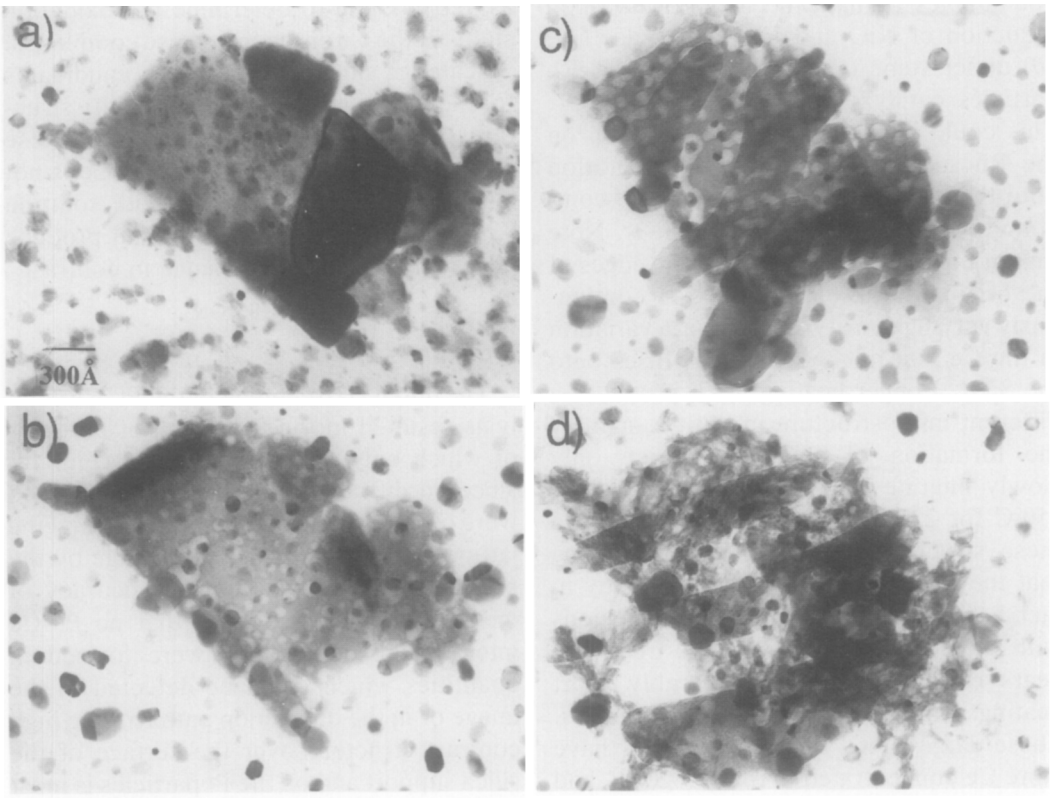

FIG. 8. Same large particle shown in the center of Fig. 7d after a series of H_2 treatments. (a) After heating in O_2 but before heating in H_2. (b) After heating in H_2 for 20 hr at 600°C. Most of the fine structure has disappeared except in the large particle and voids have formed in the large CeO_2 particle around Rh particles. (c) After heating in H_2 for an additional 58 hr at 650°C. The large CeO_2 particle has started to disperse into amorphous fingers. (d) After heating in H_2 for an additional 22 hr at 750°C. The large particle is still not completely dispersed. The fingers are still observed after heating for 100 hr total in H_2 at 600–750°C.

ticle.Through-focus imaging and the fact that unoxidized Rh is observed indicates that the CeO_2 is on top of the Rh, which is probably in contact with the SiO_2.

Figure 8 shows the transformations in microstructure of the large particle in Fig. 7d for a sequence of heat treatments in H_2. Micrographs 8b through 8d are after heating in H_2 for 20 hr at 600°C, after another 58 hr at 650°C, and after an additional 22 hr at 750°C, respectively.

In H_2, the CeO_2 begins to redisperse out onto the SiO_2 as noted previously, and within 20 hr at 600°C all CeO_2 particles less than 200 Å across (particles near the edges of the micrographs in Fig. 7) have *completely disappeared*. However, larger CeO_2 particles disperse much more slowly such that considerable Ce is present as large particles even after a total of 100 hr reduction at 600–750°C.

The first change noted upon H_2 reduction is the formation of *holes* in the CeO_2 layer, and most of these holes are *around Rh particles*. From the micrographs it is not possible to determine whether these are holes or bubbles; from the microstructures and because the film is very thin, we believe these are

not bubbles as have been observed upon reduction of NiO and Fe_2O_3 particles (*19, 20*) under some conditions. Evidently, Rh particles catalyze the reduction of CeO_2. This could occur by H_2 chemisorption on the Rh surface followed by its migration onto the CeO_2 and reduction to a Ce compound which migrates onto the SiO_2. Note that in Fig. 8b the regions near the edges of the original large particle have a continuously varying density, suggesting a variation in the Ce film thickness as it diffuses onto the SiO_2. Longer heating in H_2 produces a different microstructure in the Ce, namely the formation of "fingers" which only slowly migrate onto the SiO_2. Heating at 750°C for 22 additional hr does not cause these structures to disappear, suggesting that they are extremely stable and may in fact be equilibrium structures. In regions with smaller CeO_2 particles, the Ce disappears completely after comparably short heating times and lower temperatures. These large CeO_2 particles should have more Ce concentrated in these regions, and the observed structures are evidently associated with high Ce loadings. Note that the original sample, Fig. 7a, shows no observable evidence of Ce upon initial heating of the $Ce(NO_3)_3$ to even 600°C: the Ce appears to be distributed evenly over the entire SiO_2 film.

The fingers in Figs. 8c and 8d have sharp edges and uniform thickness. The larger ones are ~1000 Å across while the smaller are only 10 Å across. The smaller ones have nearly constant widths and can be described as needles. These needles frequently appear to emanate from Rh particles. These Ce structures are also very thin as were the initial CeO_2 structures.

We suggest that these stable structures associated with reduction of large particles of CeO_2 are some type of chemical complex between Ce and SiO_2 possibly containing some Rh. We found no complex between Ce, Rh, and Si whose diffraction pattern matches the observed patterns, and it is not as yet possible to determine the oxidation states of the Ce or the Si in these complexes. Silicates or silicides are obvious candidates for these very stable and low-mobility structures. Note that the sharp edges of these structures argue strongly that the Ce is not simply forming a surface or bulk solution with the SiO_2 because this should produce edges with continuous change in contrast.

DISCUSSION

Platinum–Cerium

The initial H_2 treatment of the Pt–Ce catalysts resulted in the formation of particles of which only Pt was crystalline (Fig. 1a) since no diffraction lines other than fcc Pt were observed (for the loading used) and the lattice constant of Pt did not change by the presence of Ce to within the accuracy of measurement. This implies that no Pt–Ce intermetallic compounds were formed in quantities which could be detected in the image or in the diffraction pattern. The high contrast structure over the surface of the silica support and on the Pt particles is most probably due to Ce as some amorphous oxide or hydride. The fact that the Pt particles were round and did not exhibit the characteristic cube shape of pure Pt particles formed under similar conditions argues that the Ce species is present on the surface of the Pt.

Treatment in O_2 resulted in the formation of CeO_2. The argument that the Ce species was distributed over the surface of the silica is substantiated by the increase in contrast of the structure on the silica surface as particles of CeO_2 are formed and by the ability to identify and locate this structure as CeO_2 through dark field imaging (Fig. 2b). We have shown previously (*12*) that noble metal oxides wet silica more than their parent metals and as a result spread out more on the silica surface than the metals. This size reduction is probably the result of an overlayer of the Ce species which spreads out over the support forming the rectangular oxide structures on the support at the expense

of the larger particles, a consequence of the CeO_2 wetting the support more than the Pt (Fig. 2a).

Upon reduction of the oxidized samples (Fig. 2c), the Pt particles do not return to their original size. This could arise from Ce in the original particles or from a difference in height of the particles after the heat treatment. The CeO_2 on the silica surface was replaced by very small (~10 Å) particles which were uniformly distributed on the silica surface. After prolonged heating in H_2 (Fig. 2d), the Ce formed larger crystalline particles which produced rings in the diffraction pattern that can be assigned as CeH_2. This determination is substantiated by additional experiments on samples with a higher loading of Ce as noted above and by the fact that all rare earth metals are known to readily form dihydrides in 1 atm of H_2 (*21, 22*). Confirmation of the presence of crystalline Ce hydride and the fact that through-focus micrographs show the Ce species to be on top of the Pt particles suggest that the Ce species present as a result of the initial H_2 treatment was in fact an amorphous Ce hydride. It is possible that some of the Ce reacts with the support to form a silicate or a silicide.

No significant difference was observed in the particle size distribution of the Pt–Ce with respect to those of pure Pt (*11*) nor did we see any evidence of any change in thermal stability with respect to sintering of these samples as reported for Pt-Ce/Al_2O_3 (*9*). It does appear, however, that Ce as the oxide or the hydride remained highly dispersed over the substrate throughout the $H_2 \rightarrow O_2 \rightarrow H_2$ treatment sequence since only after samples had undergone this treatment sequence were detectable amounts of crystalline CeH_2 observed.

The idealized morphology of Pt–Ce is shown in Figs. 9a and 9b. After heating in a reducing environment, Ce is present as an amorphous film covering the SiO_2 and the Pt particles. The film, which may be CeH_2, reduces the anisotropy in the surface energies of the Pt, and the particles are more rounded than observed for Pt-only. Heating Pt–Ce in O_2 oxidizes the Ce to CeO_2 while the Pt particles are nearly unchanged. The CeO_2 forms lower contrast rectangular particles adjacent to Pt particles and also forms ~25 Å particles which are distributed over the support. Treatment in H_2 again returns the system to the microstructure observed after the initial H_2 treatment.

Rhodium–Cerium

The idealized microstructure after treatment in H_2 of Rh–Ce samples with high Ce loadings prepared by addition of Ce from salt is shown in Fig. 9c. The Rh particles are rounded and no longer assume the characteristic hexagonal structure of Rh-only. Only when Ce is present in large amounts ($Ce/Rh \geq 2.5$) are detectable amounts of the CeRh intermetallic observed. At lower Ce loadings ($Ce/Rh < 1$) and in samples where Ce was added by vacuum evaporation, it appears that H_2 inhibits the formation of any crystalline Rh–Ce intermetallic compounds because diffraction rings assignable to a Rh–Ce intermetallic were not observed in these samples.

We suggest that, as in the Pt–Ce/SiO_2 system, Ce hydride may be formed preferentially in H_2 instead of any intermetallic compounds. Also, analogous to the Pt–Ce system, a phase assignable as CeH_2 which can be seen as the fine high-contrast structure throughout the sample (Fig. 6a) is uniformly distributed on the surface of the silica as well as the Rh particles.

Treatment of samples with $Ce/Rh \geq 2.5$ formed large CeO_2 particles and needles (Fig. 7d) as shown in Fig. 9d. Heating in O_2 also resulted in the formation of Rh_2O_3. However, some unoxidized Rh metal remained, under conditions where Rh alone was fully converted to Rh_2O_3 (*12*) indicating that Ce inhibits oxidation of Rh. Heating

samples with Ce/Rh < 1 in oxygen at 550°C transformed the fine high contrast structure into ~50 Å CeO_2 particles (Fig. 6b), like that of the Pt–Ce system (Fig. 2a), confirming the distribution of Ce over the surface of the support. This result is in agreement with the CeO_2 particle size found in Rh–Ce/Al_2O_3 by Oh[23] using X-ray diffraction.

Subsequent treatment of the oxidized samples in H_2 resulted in the formation of amorphous phases and small crystalline Ce hydride particles. The disappearance of many of the small particles after the $H_2 \rightarrow O_2 \rightarrow H_2$ sequence was accompanied by a decrease in the intensity of the CeRh rings in the diffraction pattern. This indicates that Ce hydride is formed at the expense of CeRh and that Ce hydride is the more stable species under these conditions, further substantiating the hypothesis that Ce hydride was present in all reduced samples. We suggest that the majority of the Ce in the reduced samples may be present as an amorphous film of Ce hydride over the surface of the support and Rh particles.

Some differences in microstructure were observed between the two methods of Ce addition. In samples where Ce was added by vacuum evaporation, crystalline Rh metal, Ce metal and a hydride assignable as $CeH_{2.53}$ were observed in the samples containing both Rh and Ce, but only an amorphous film was observed in samples with Ce-only. This suggests that Rh promotes the crystallization of Ce. No intermetallic compounds were detected in these experiments, further indicating that formation of Ce hydride is preferred over formation of Rh–Ce alloys.

Treatment of the Ce-only sample in oxygen at 600°C resulted in the formation of ~50 Å CeO_2 particles (Fig. 3b) similar to those observed for samples with low Ce loadings prepared from the salt. The behavior of Ce is different, however, when Rh is present (Fig. 9d). Large crystals of CeO_2 (up to ~200 times larger than in the sample without Rh) formed on top of unoxidized Rh indicating that Rh catalyzes Ce oxidation. The amount of Rh observed appears to be less than before oxidation, suggesting that some Rh may form an amorphous oxide or mixed oxide.

Subsequent treatment of the oxidized samples in H_2 resulted in reduction of most of the CeO_2 particles and the formation of highly twinned Rh particles. The larger CeO_2 particles dispersed more slowly and may form a stable complex with the SiO_2 support. The Rh particles were redistributed by the $H_2 \rightarrow O_2 \rightarrow H_2$ sequence and approximately equal particle sizes were observed for all three Rh loadings (Figs. 3f, 4c, and 4f). This indicates that dispersion of Rh when Ce is present is sensitive to H_2–O_2 cycling. The amorphous Ce film was still observed after the second treatment in H_2 and we suggest that the majority of the Ce present in the reduced samples was as a film of Ce, reduced oxide, or Ce hydride covering the surface of the support and Rh particles.

RATES: EXPERIMENTAL

Rh–Ce catalysts were prepared from aqueous solutions of $RhCl_3 \cdot 3H_2O$ and $Ce(NO_3)_3 \cdot 3H_2O$ supported on Aerosil 200 silica. Three catalysts with different Ce loadings were prepared to study ethane hydrogenolysis. One had 5% Rh and no Ce. The other two were coimpregnated to yield 5% Rh/1.25% Ce and 5% Rh/5% Ce, respectively. In each case, the resulting slurry was dried overnight at 100°C in N_2 and then calcined for 4 hr at 650°C in O_2.

Three catalysts were also prepared to study CO hydrogenation. The first two were prepared as described above by impregnation to yield 5% Rh and 5% Rh/5% Ce. A third catalyst was made to investigate the effect of Ce on the dispersion of Rh. This was done by impregnating Ce on a *calcined* Rh catalyst in which the Rh has already been dispersed to give a final loading of 5% Rh and 5% Ce. This 5% Rh/post 5% Ce catalyst was then dried and calcined again. A blank of 5% Ce was also prepared and showed

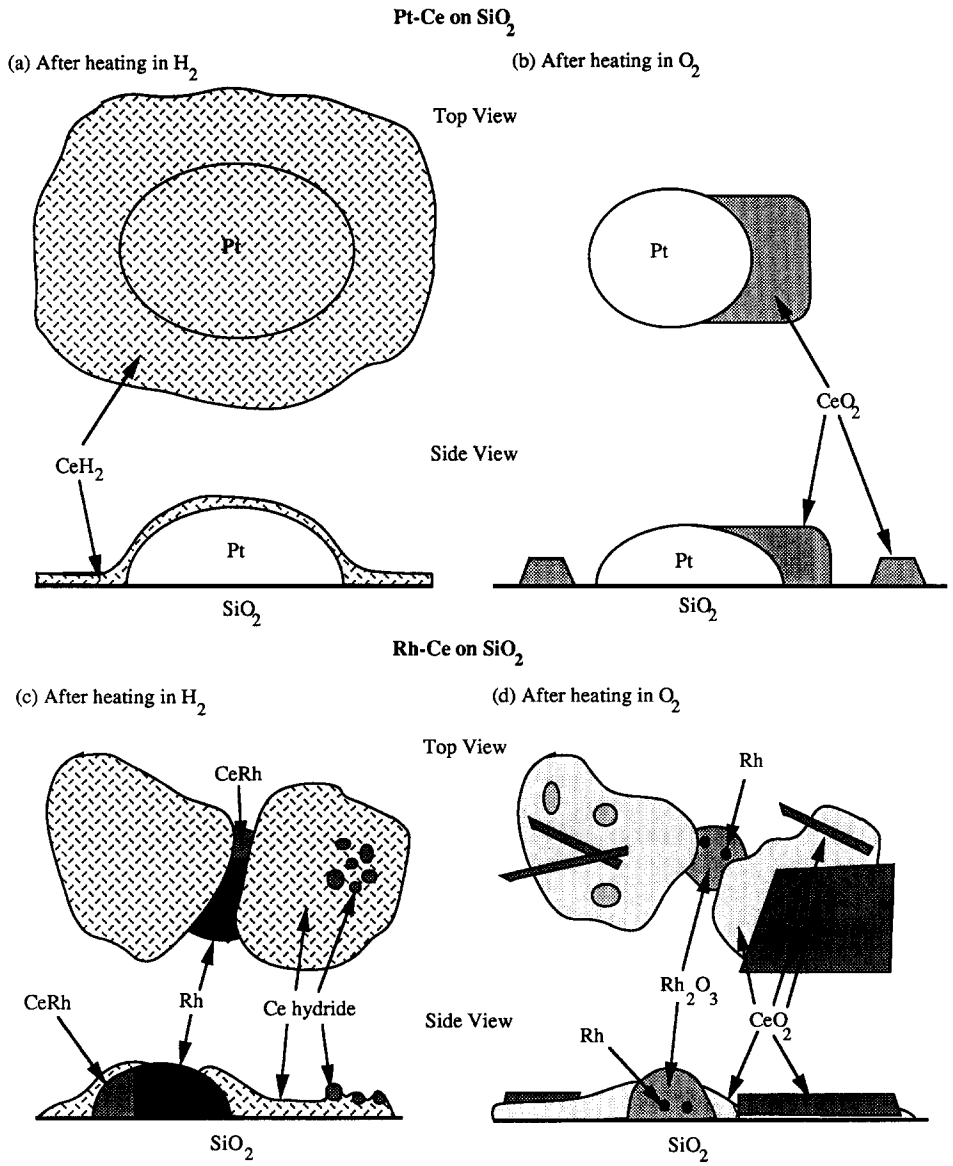

FIG. 9. Illustrations of the idealized morphologies of Pt–Ce and Rh–Ce on SiO_2 after reducing and oxidizing heat treatments. (a) Treatment of Pt–Ce samples in H_2 results in the formation of round highly twinned Pt particles. Amorphous CeH_2 is also formed and covers the surface of the silica as well as the Pt particles. (b) Treatment of Pt–Ce in O_2 causes the oxidation of Ce to CeO_2 which forms as rectangular structures adjacent to the Pt particles and as ~25Å particles distributed over the support. (c) Rh–Ce for high Ce loadings (Ce/Rh $\geq$ 2.5) prepared by addition of Ce from the salt. After heating in H_2, CeRh particles are observed in addition to Rh and CeH_2. The CeRh intermetallic is not observed at lower Ce loadings or in samples where Ce was added by vacuum evaporation. (d) After heating in O_2, the Ce oxidizes to form large CeO_2 particles and needles, while Rh partially oxidizes to Rh_2O_3.

negligible activity for both ethane hydrogenolysis and CO hydrogenation.

Kinetic studies were done in an atmospheric pressure microreactor and gas chromatograph (GC) as described elsewhere (*24*). Premixed 3% C_2H_6/21% H_2/76% He was used for ethane hydrogenolysis, and the flow rate of ethane through the atmospheric

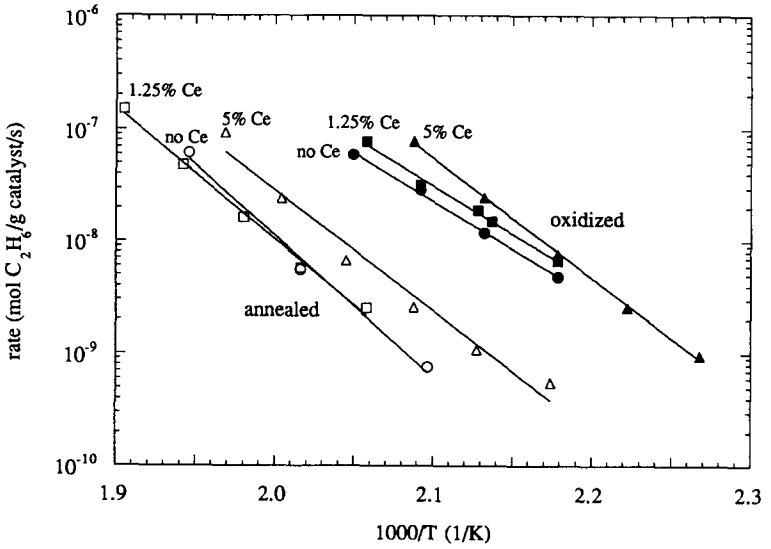

FIG. 10. Arrhenius plot for ethane hydrogenolysis by 5% Rh/Ce on SiO_2. Ce loadings are indicated on figure. Open symbols indicate reduced catalysts, and solid symbols indicate oxidized catalysts.

pressure reactor was about 1 cc/min. For CO hydrogenation, ultra-high-purity H_2 and CO were fed to the reactor in a 3/1 H_2/CO ratio at a total flow of about 10 cc/min. Conversions of ethane and CO were kept below ~5% to ensure that we observed differential kinetics. Standard mixtures of C_1–C_6 alkanes and $C_{2=}$–$C_{6=}$ alkenes were used for GC calibration and the locations of the CH_3OH and C_2H_5OH peaks were identified. However, sensitivities were not calibrated and were assumed to be identical to CH_4 for qualitative comparisons.

About 200 mg of the catalyst was transferred to the reactor for experiments. The calcined catalyst was first annealed for 4 hr at 650°C, and then rates were measured. The samples were then oxidized at 650°C, followed by low-temperature reduction at 300°C, and the rates were measured again. These are called the annealed and oxidized states of the catalyst.

RESULTS

Ethane Hydrogenolysis

An Arrhenius plot comparing the rates of ethane hydrogenolysis on 5% Rh, 5% Rh/1.25% Ce, and 5% Rh/5% Ce is shown in Fig. 10. It can be seen from this plot that the addition of Ce increases the reaction rate slightly and that the increase is nearly the same following both the reducing and oxidizing pretreatments. The activity increases with increasing Ce loading up to a factor of ~3 for the highest Ce loading studied.

The rate of ethane hydrogenolysis is thus more sensitive to catalyst pretreatment than to Ce addition. All three catalysts are ~25 more active after oxidation than after reduction, and the increase is roughly independent of Ce loading. The slopes of the curves in Fig. 10 do not differ significantly. The activation energies observed were about 50–65 kcal/mole and were slightly lower after oxidation than after reduction.

CO Hydrogenation

An Arrhenius plot comparing the rates of CO hydrogenation by 5% Rh, 5% Rh/5% Ce, and 5% Rh/post 5% Ce is shown in Fig. 11. The rate of Co consumption increases significantly after the addition of 5% Ce. The plot shows that the rate after addition of Ce

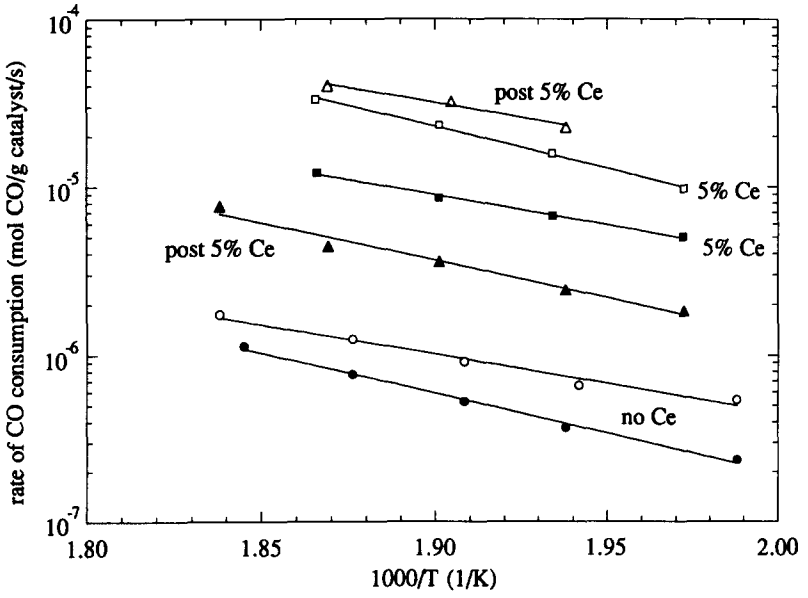

FIG. 11. Arrhenius plot for CO consumption by 5% Rh/Ce on SiO_2. Ce loadings are indicated on figure. Open symbols indicate reduced catalysts, and solid symbols indicate oxidized catalysts.

is ~12 times greater in the reduced state and ~30 times greater in the oxidized state than the rate without Ce.

It is possible that the addition of Ce might alter the dispersion of Rh on SiO_2. The results from the 5% Rh catalyst that was impregnated with Ce after the Rh had been previously dispersed indicate that this is at most a minor effect. Comparison of the rates of the co- and postimpregnated catalysts shows a slight difference in sensitivity to pretreatment in H_2 and O_2, but the rates are nearly equal to within experimental error.

Figure 11 also shows that the rate of CO consumption by the annealed 5% Rh and 5% Rh/5% Ce catalysts increases by only a factor of ~2 after oxidation. For the conditions studied, this reaction is therefore more sensitive to the addition of Ce to Rh than to pretreatment of the catalyst in H_2 or O_2. This result is opposite to that observed for ethane hydrogenolysis. The activation energy for CO consumption was 16–23 kcal/mole for all three catalysts and both pretreatments.

Unlike ethane hydrogenolysis, CO hydrogenation can produce many products including alkanes, alkenes, and oxygenates. We investigated the effects of Ce addition and H_2 and O_2 pretreatments on selectivity. No significant differences in selectivity were observed between the co- and postimpregnated 5% Rh/5% Ce catalysts. Only the results from the postimpregnated catalyst will be discussed since data was obtained over a wider temperature range.

Arrhenius plots of the observed products are shown in Fig. 12 after reduction pretreatment and in Fig. 13 after oxidation. Comparison of the two annealed catalysts shows that the addition of Ce increases the rates for formation of higher molecular weight products more than it increases the rate of CH_4 formation. The rate of C_3H_6 production increased more than the rates of the other alkanes after the addition of Ce. Comparison between the two oxidized catalysts in Fig. 13 shows the same differences as the reduced catalysts. We identified the location of the MeOH peak and, assuming a response

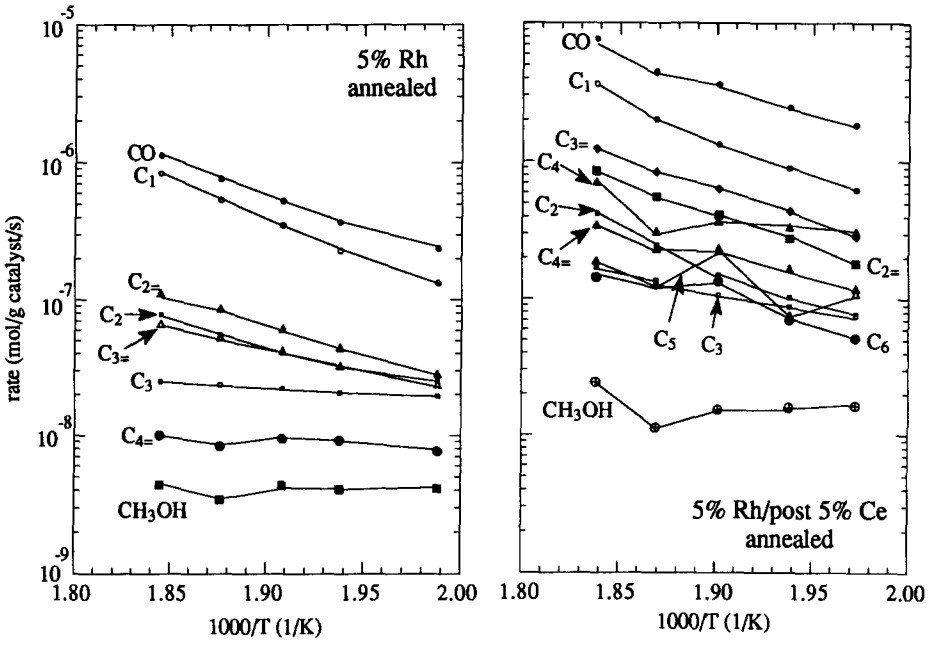

FIG. 12. Arrhenius plot showing rates of formation of observed products for CO hydrogenation by annealed 5% Rh/Ce on SiO_2.

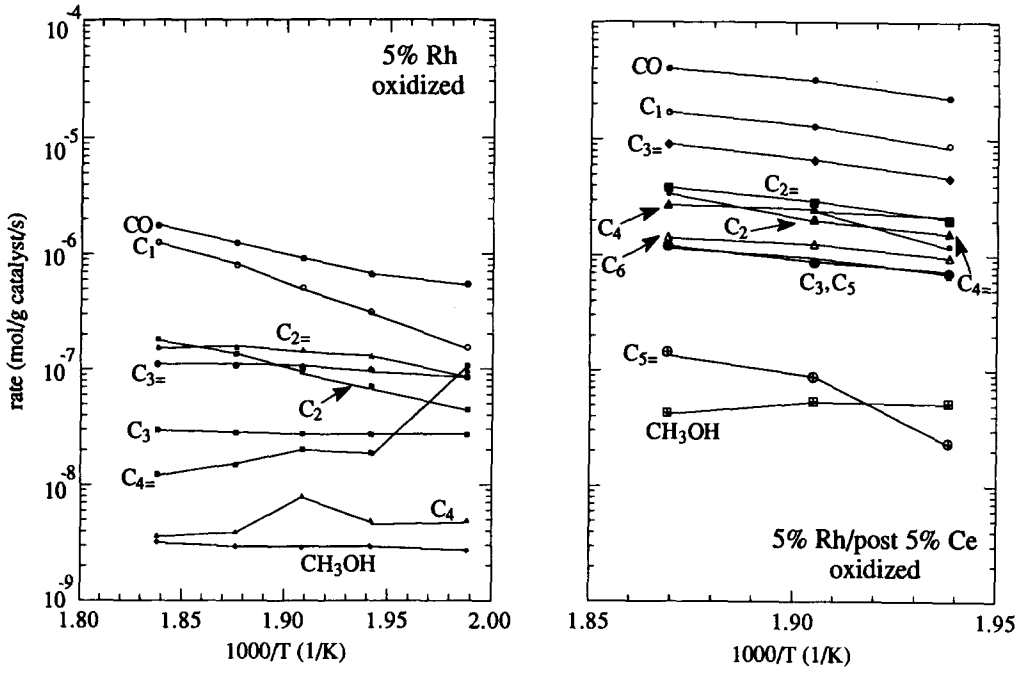

FIG. 13. Arrhenius plot showing rates of formation of observed products for CO hydrogenation by oxidized 5% Rh/Ce on SiO_2.

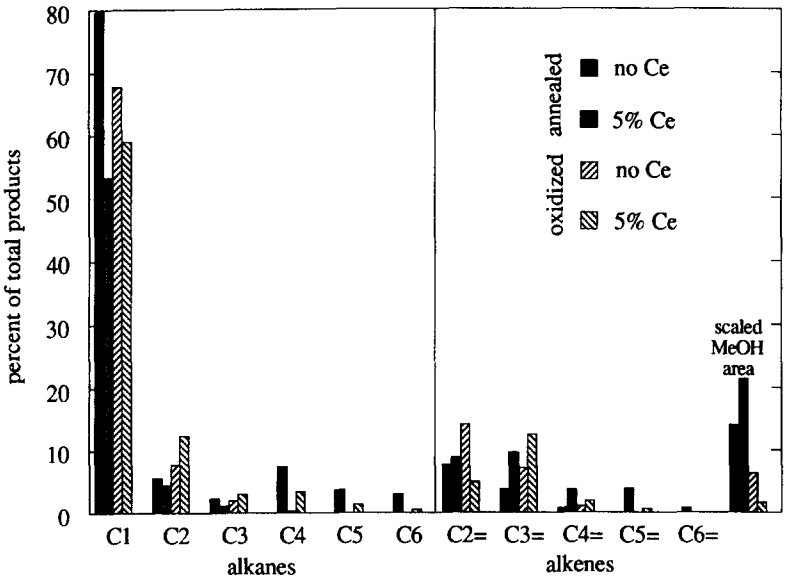

FIG. 14. Observed product distributions for CO hydrogenation at 243°C by 5% Rh and 5% Rh/post 5% Ce on SiO_2. The selectivities of 5% Rh/5% Ce and 5% Rh/post 5% Ce were equal to within experimental error. Addition of Ce shifted selectivity toward higher molecular weight products.

factor identical to methane, calculated a rate to compare catalysts and pretreatments. The rate of MeOH formation apparently changes by less than ~3 between treating in H_2 or O_2 but increases by about an order of magnitude after Ce addition.

Figure 14 compares the product distribution at 243°C. This figure shows that ~25% less methane is formed when Ce is added and that the selectivity shifts toward higher alkanes and alkenes as noted above. The total fraction of alkanes formed after pretreatment in H_2 increases from ~10% to ~25% when 5% Ce is added to 5% Rh/SiO_2. After oxidation, both catalysts formed ~20% alkanes. More MeOH was produced when Ce was added to Rh in the annealed state, but the reverse was observed in the oxidized state. Both catalysts formed at least twice as much MeOH after pretreatment in H_2 than after treatment in O_2.

CORRELATION OF MICROSTRUCTURE AND REACTIVITY

To summarize reactivity measurements, ethane hydrogenolysis rates on Rh/SiO_2 are increased slightly (less than a factor of three) by addition of up to 5% Ce, but the activity is higher by a factor of ~50 after the catalyst has been treated in O_2, with or without Ce added. Thus, Ce has a small promotion effect in this reaction. In contrast, CO hydrogenation rates are very strongly increased by addition of Ce (factor of >20), but in this reaction pretreatment in H_2 or O_2 has less influence on the rate.

These results are consistent with the effect of H_2 and O_2 treatments on pure Rh and other metals supported on SiO_2 which were reported previously for alkane hydrogenolysis (*24*) and for CO hydrogenation (*25*). The interpretations of these results was that treatment in O_2 at ~600°C produces microcrystalline Rh_2O_3 which upon low temperature reduction in H_2 forms 10–20 Å crystallites of Rh metal; annealing in H_2 at ~600°C sinters these back into larger single crystal particles. We showed by H_2 chemisorption that the surface areas of the oxidized particles were increased by only a factor of ~2 so that the variations in activity and selectivity in alkane hydrogenolysis are caused pri-

marily by a change in catalyst activity rather than surface area. We speculated that this was due to the higher reactivity for this reaction on low coordination sites formed on the microcrystalline metal particles.

The TEM images suggest that Ce causes little variation in the geometric areas of metal particles, and the differences in reactivity between coimpregnated and postimpregnated Ce confirms that Ce retardation of Rh sintering is not a major effect, although it increases the defect density in the Rh particles. Ce may be expected to simply cover some of the Rh surface, especially in O_2 which causes Ce to coalesce around metal particles. Evidently, any covering of metal sites is more than compensated by the increase in activity in the presence of Ce.

Further evidence that Ce produces a change in activity rather than surface area comes from the large alteration it produces in reaction selectivity of CO hydrogenation, with much more higher hydrocarbons and olefins produced with Ce.

The alteration in activity and selectivity of CO hydrogenation by Ce seems to be remarkably uncorrelated with the drastic alteration of microstructures between heating in H_2 and O_2. Even though the surface is altered strongly on a 10 to 1000 Å scale, the local sites and their densities on which the CO hydrogenation reaction occurs are evidently unchanged. This could be because the active sites are not associated with the large Rh particles at all but rather occur on smallar particles or isolated Rh atoms which are invisible to TEM. Another interpretation which we prefer is that, even though the microstructures are quite different after H_2 or O_2 treatments, immediately upon treatment in a CO + H_2 mixture, the surfaces are transformed by the presence of H_2O into an "oxidized" state. That is, we suspect that H_2O, a product of the reaction, can transform the surface layer of Rh particles into a rough surface with low coordination sites whose structure is independent of whether the surface had previously been treated in H_2 or O_2.

In summary, these results show that, while microstructures of Rh particles with Ce added are changed markedly by different pretreatments, the effect of pretreatment conditions on CO hydrogenation rates is quite small, although Ce is an efficient promoter. In contrast, pretreatment strongly affects ethane hydrogenolysis, but the rate is fairly insensitive to the large changes in microstructure produced by Ce addition.

SUMMARY

This study shows that Ce does not interact strongly with Pt and Rh particles supported on amorphous silica in strongly reducing conditions. We saw no evidence for the formation of any intermetallic in the Pt–Ce system, but we observe detectable amounts of the intermetallic compound CeRh for higher Ce loadings, Ce/Rh > 2.5. Ce was present on the surface of both the silica support and the noble metals as a hydride when treated in H_2 and as CeO_2 when treated in O_2. Evidently, the presence of Ce as either a hydride or oxide on the surface of the noble metal particles alters their equilibrium shapes and increases internal defect densities. Ce increases the temperature at which Rh is oxidized, presumably also by covering the Rh particles and protecting them against oxidation.

The TEM results suggest that Ce should increase defect densities, may form intermetallic compounds under strongly reducing conditions, and may cover metal particles under oxidizing conditions. We emphasize that these results are on fairly large particles under strongly oxidizing or reducing conditions at high temperatures. Structures of smaller particles under milder conditions can only be speculated from these experiments.

Extensive heating and cycling in H_2 and O_2 produces very stable structures which do not disappear even after heating for many hours at 750°C. We suspect that these involve Ce, Rh, and SiO_2 complexes, but all are amorphous. Various chemical

and microscopic techniques are now being used to attempt to identify these structures.

Ce causes a slight increase in activity of Rh for ethane hydrogenolysis and a marked improvement in activity and selectivity for CO hydrogenation. While microstructures of Rh particles change significantly by addition of Ce and by treatment in H_2 or O_2, we have no simple explanation for the relationship between microstructure and catalytic activity. Reaction properties are determined by local atomic configurations at surfaces which are not necessarily evident in TEM.

REFERENCES

1. Taylor, K. C., *in* "Catalysis Science and Technology" (J. R. Anderson and M. Boudart, Eds.), Vol. 5, Springer-Verlag, 1984.
2. Schlatter, J. C., and Mitchell, P. J., *Ind. Eng. Chem. Prod. Res. Dev.* **19,** 288 (1980).
3. Herz, R. K., and Sell, J. A., *J. Catal.* **94,** 166 (1985).
4. Kiennemann, A., Breault, R., Hindermann, J.-P., and Laurin, M., *J. Chem. Soc., Faraday Trans. 1* **83,** 2119 (1987).
5. Underwood, R. P., and Bell, A. T., *Appl. Catal.* **21,** 157 (1986).
6. Underwood, R. P., and Bell, A. T., *Appl. Catal.* **34,** 289 (1987).
7. Yung-Fang, Y. Y., *J. Catal.* **87,** 152 (1984).
8. Solymosi, F., Pasztor, M., and Rakhely, G., *J. Catal.* **110,** 413 (1988).
9. Summers, J. C., and Ausen, S. A., *J. Catal.* **58,** 131 (1979).
10. Hamilton, J. F., *J. Appl. Phys.* **39,** 5333 (1968).
11. Wang, T., Lee, C., and Schmidt, L. D., *Surf. Sci.* **163,** 181 (1985).
12. Lee, C., and L. D. Schmidt, *J. Catal.* **101,** 123 (1986).
13. Lee, C., Schmidt, L. D., Moulder, J. F., and Rusch, T. W., *J. Catal.* **99,** 472 (1986).
14. Grove, C., and Schmidt, L. D., *Appl. Surf. Sci.* **35,** 199 (1988).
15. Pearson, W. B., "Handbook of Lattice Spacings and Structures of Metals," Vol. 2, pp. 1403–1405. Pergamon, New York, 1967.
16. Tellefsen, M., Kaldis, E., and Jilek, E., *J. Less Common Met.* **110,** 107 (1985).
17. "The Handbook of Binary Phase Diagrams." General Electric, 6/1978.
18. Chojnacki, T. P., Ph.D. thesis, University of Minnesota, 1989.
19. Lee, C., and Schmidt, L. D., *J. Electrochem. Soc.* **136,** 2471 (1989).
20. Engell, H., and Wever, F., *Acta Metall.* **5,** 695 (1957).
21. "Hydrogen in Metal" (G. Alefeld and J. Volkl, Eds.), Vol. 1, p. 175. Springer-Verlag, 1978.
22. Libowitz, G. G., and Maeland, A. J., *in* "Handbook on the Physics and Chemistry of Rare Earths" (K. A. Gschneidner, Jr. and L. Eyring, Eds.), Vol. 3, North–Holland, 1979.
23. Oh, S. H., and Eickel, C. C., *J. Catal.* **112,** 543 (1988).
24. Gao, S., and Schmidt, L. D., *J. Catal.* **111,** 210 (1988).
25. Gao, S., and Schmidt, L. D., *J. Catal.* **115,** 356 (1989).